NOVA SCHOOL OF SCIENCE & TECHNOLOGY

DEPARTAMENT OF
Material Science

Michele dell'Erba

BSc in Micro and Nanotechnology Engineering

Multi-layer memristors for large-scale artificial neural network application

MASTER IN Micro and Nanotechnology Engineering

NOVA University Lisbon

September, 2024

DEPARTAMENT OF
Material Science

Multi-layer memristors for large-scale artificial neural network application

Michele dell'Erba

Master in Micro and Nanotechnology Engineering

Adviser: Jonas Deuermeier
Assistant Researcher, *NOVA University Lisbon*

Co-advisers: Asal Kiazadeh
Assistant Researcher, NOVA University Lisbon

Examination Committee:

Chair: Pedro Miguel Cândido Barquinha
Associate Professor, FCT-NOVA

Rapporteurs: Joana Maria Dória Vaz Pinto Morais Sarmento
Assistant Professor, FCT-NOVA

Adviser: Jonas Deuermeier
Assistant Researcher, FCT-NOVA

MASTER IN Micro and Nanotechnology Engineering

NOVA University Lisbon
October 2024

Multi-layer memristors for large-scale artificial neural network application

ACKNOWLEDGMENTS

I would like to express my deepest gratitude to my family and friends for their unwavering support and encouragement throughout this journey. Their belief in my potential and constant motivation gave me the strength to overcome challenges and strive for excellence. I would like to express my deepest gratitude to my girlfriend, Cátia, for her unwavering support, patience, and encouragement throughout this entire journey.

My sincere appreciation goes to my advisors, Professor Jonas Deuermeier and Dr. Asal Kiazadeh, for their exceptional guidance, mentorship, and patience. Your expertise and insights have been fundamental to the completion of this work, and I am immensely grateful for the opportunities you provided to learn and grow as a researcher. Your encouragement and constructive feedback have been instrumental in shaping my academic journey.

I also extend my gratitude to CENIMAT and the Associate Laboratory Institute of Nanostructures, Nanomodelling, and Nanofabrication – i3N, for providing the infrastructure and resources necessary for my research. This work was financed by national funds from FCT - Fundação para a Ciência e a Tecnologia, I.P., in the scope of the project's LA/P/0037/2020, UIDP/50025/2020, and UIDB/50025/2020. The support and funding from FCT made this work possible, and I am deeply appreciative of their contribution to advancing scientific research in this field.

ABSTRACT

This study investigates the fabrication, electrical characterization, and optimization of Al_2O_3-based memristor devices using various electrode materials and configurations. The devices were constructed with different top contacts (Al, Ag, Cu, Ti/Au) and bottom electrodes (AZO, Mo, Ti/Pt) combined with Al_2O_3 switching layers deposited via Atomic Layer Deposition (ALD). Initial tests demonstrated that the device's switching behaviour was influenced by the electrode material and the thickness of the switching layer. Devices with Ag and Cu top electrodes demonstrated better switching performance compared to those with Al or Ti/Au electrodes, attributed to the formation of stable conductive filaments.

To further enhance device performance and reliability, argon plasma treatment was applied to the switching layer. However, the treatment failed to significantly improve switching properties, leading to inconsistent device performance and reduced stability. While an asymmetric defect profile was achieved by adding a sub stoichiometric AlO_x layer between the Al_2O_3 and the top electrode improving defect density control and contributing to more stable filament formation and dissolution

The final Pt/Al_2O_3/AlO_x /Cu configuration showed improved stability and switching performance, making it a promising candidate for non-volatile memory applications. These results highlight the importance of electrode selection, layer thickness control, and defect engineering in optimizing Al_2O_3-based memristors for potential applications in non-volatile memory technologies.

Keywords: Al_2O_3-based memristor; AlO_x defect layer; Argon plasma treatment; ALD

RESUMO

Com este trabalho pretende-se investigar a fabricação, caracterização elétrica e otimização de memristores baseados em Al_2O_3, utilizando vários materiais e configurações. Os dispositivos foram criados com diferentes contatos superiores (Al, Ag, Cu, Ti/Au) e elétrodos inferiores (AZO, Mo, Ti/Pt), combinados com camadas ativas de Al_2O_3 depositadas via *Atomic Layer Deposition* (ALD). Os testes iniciais mostraram que a escolha do elétrodo e a espessura da camada de ativa influenciaram fortemente o comportamento dos dispositivos. Dispositivos com elétrodos superiores de Ag e Cu exibiram melhor *electroforming* em comparação com aqueles com elétrodos de Al ou Ti/Au, devido à formação de filamentos condutores mais estáveis.

Para melhorar o desempenho dos dispositivos aplicou-se um tratamento com plasma de argon na camada de Al_2O_3. No entanto, o tratamento não melhorou significativamente as propriedades de *switching*, resultando num desempenho inconsistente. A introdução de um perfil assimétrico de defeitos, por meio da adição de uma camada subestequiométrica de AlO_x entre o Al_2O_3 e o elétrodo superior, melhorou o controle da densidade de defeitos e contribuiu para a formação e dissolução mais estável dos filamentos.

A configuração final, consistindo em uma estrutura $Pt/Al_2O_3/AlO_x$ /Cu, mostrou estabilidade e desempenho da *switching layer*. Esses resultados destacam a importância da seleção de elétrodos, controle da espessura das camadas e engenharia de defeitos na otimização de memristores baseados em Al_2O_3 para aplicações em tecnologias de memória.

Palavras chave: Al_2O_3 memristor; AlO_x; Tratamento com plasma de Árgon; ALD

CONTENTS

1 STATE OF THE ART 1

1.1 History of The Memristor 1

1.2 Resistive Switching Mechanism 2

1.2.1 Electrochemical Metallization Cell (ECM) 2

1.2.2 Valence Change Mechanism 3

1.2.3 Unipolar Physical Switching Effects 4

1.2.4 Threshold Switching 5

1.3 Atomic Layer Deposition 6

1.4 Aluminium Oxide Switching Layer By ALD 6

2 METHODS AND MATERIALS 8

2.1 Device Fabrication 8

2.1.1 Substrate Preparation 8

2.1.2 Bottom Contact 8

2.1.3 Switching Layer 8

2.1.4 Top Contact 9

2.1.5 Fully patterned devices 9

2.2 Electrical And Chemical Characterization 10

3 RESULTS AND DISCUSSION 11

3.1 AZO/ Al_2O_3 11

3.1.1 TiAu And Al Top Contact 12

3.1.2 TiAg And Ag Top Contacts 13

3.2 Al_2O_3 With Argon Plasma Treatment 14

3.2.1 AZO/ Al_2O_3/Cu 15

3.2.2 Mo/ Al_2O_3/Cu 17

3.3 Defective AlO_x and bilayers 19
3.3.1 X-ray Photoelectron Spectroscopy 19
3.3.2 Pt/ AlO_x (150ºC/300ºC) Cu 21
3.3.3 Pt/ Al_2O_3 AlO_x (300ºC) /Cu 22
3.3.4 Pt/ $Al_2O_3AlO_x$ (150ºC)/Cu 23
4 CONCLUSIONS AND FUTURE PERSPECTIVES 27
4.1 Conclusions 27
4.2 Future Perspectives 27
5 BIBLIOGRAFIA 29

LIST OF FIGURES

Figure 1-1 Relationship between the four fundamental circuit elements 1
Figure 1-2 Steps for the creation of the filament and curve comparison[8] 3
Figure 1-3 Valence change formation[6] 4
Figure 1-4 Unipolar and bipolar classic curves [4] 5
Figure 3-1 **(a)**Pristine curves for devices with Ag and TiAg as top contact, with 5 and 10 nm switching layer thickness **(b)** Pristine curves for devices with Al and TiAu as top contact, with 5 and 10 nm switching layer thickness 12
Figure 3-2 (a) Switching characteristics typical behavior of AZO/ Al_2O_3 (10 nm) /TiAg (b) Switching characteristics typical behavior of AZO/ Al_2O_3 (10 nm) /Ag 13
Figure 3-3 **(a)** Switching characteristics typical behavior of AZO/Al2O3 (5 nm) /TiAg **(b)** Switching characteristics typical behavior of AZO/Al2O3 (5 nm) /Ag 14
Figure 3-4 **(a)** Pristine state of different AZO/Al_2O_3/Cu with 0 min of Argon plasma treatment devices **(b)** Pristine state of different AZO/Al_2O_3/Cu with 10 min of Argon plasma treatment devices 15
Figure 3-5 **(a)** Pristine state of different AZO/Al2O3/Cu with 20 min of Argon plasma treatment devices **(b)** Pristine of the three different times tested on the AZO/Al_2O_3/Cu samples 16
Figure 3-6 **(a)** Switching characteristic of AZO/Al2O3/Cu with 0 minutes of argon plasma treatment **(b)** Switching characteristic of AZO/Al2O3/Cu with 10 minutes of argon plasma treatment 16
Figure 3-7 Switching characteristic of AZO/Al2O3/Cu with 20 minutes of argon plasma treatment .. 17
Figure 3-8 **(a)** Pristine state of three different devices from the Mo/Al_2O_3/Cu sample with 0 minutes of argon plasma treatment **(b)** Pristine state of three different devices from the Mo/Al_2O_3/Cu sample with 10 minutes of argon plasma treatment 18
Figure 3-9 Pristine state of three different devices from the Mo/Al_2O_3/Cu sample with 20 minutes of argon plasma treatment 18
Figure 3-10 (a) shows an Al2O3 film grown with the standard process. The AlOx film grown at 300C in (b) reveals an increased amount of hydroxyl groups. This amount is further increased with a lower growth temperature of AlOx, Figure (c). The O 1s component at high 21
Figure 3-11 Pristine state of the TiPt/AlOx /Cu with the two different temperature depositions of the AlOx layer, 150ºC and 300ºC 21
Figure 3-12 Pristine map of TiPt/$Al_2O_3AlO_x$ /Cu sample with 30 um^2 area. The AlO_x deposition at 300ºC, with two different range of voltage, -0.5;0.5 and -1;1 22

Figure 3-13 **(a)** Switching characteristics of TiPt/Al2O3AlOx /Cu with the AlOx deposition at 300ºC. The device showed thresh-old behaviour repeating the set operation with both positive and negative voltage **(b)** Time to break down test, with fixed 1.2 V and 1.3 V applied to the top contact of the device 23
Figure 3-14 Pristine map of Pt/ $Al_2O_3AlO_x$ (150ºC)/Cu devices with a 30 um^2 area. The AlO_x deposition at 150ºC. 24
Figure 3-15 **(a)** Reset forming and consequent set **(b)** Retention time test after reset forming on the same device as fig. 3-15 (a) 24
Figure 3-16 **(a)** Set forming and consequent reset **(b)** Retention time test after set forming on the same device as fig 3-16 (a) 25
Figure 3-17 **(a)** Negative forming with consecutive increase of the LRS. **(b)** Unipolar device, with positive forming 25
Figure 3-18 Switching characteristics with positive forming and set and reset with opposite polarities. 26

LIST OF TABLES

Table 2-1 Summary of the device fabrication and structure 10
Table 3-1 Comparison of the results from the first two batches 19
Table 3-2 Calculations of the ratio of oxygen (bonded to aluminium) over aluminium, based on the atomic concentration of Al, C, and O as well as the O 1s fitting results 20
Table 3-3 Comparison of the results from the third batch 26

ACRONYMS

ALD - Atomic Layer Deposition
AlO_x - Aluminium Oxide (sub-stoichiometric form of Al_2O_3)
AZO - Aluminium-doped Zinc Oxide
CF - Conductive Filament
CBRAM - Conductive Bridge Random Access Memory
ECM - Electrochemical Metallization
HRS - High Resistance State
LRS - Low Resistance State
RRAM - Resistive Random Access Memory
TMA - Trimethylaluminum
VCM - Valence Change Mechanism
XPS - X-ray Photoelectron Spectroscopy
NVRS - Non-Volatile Resistive Switching
AE - Active Electrode
CE - Counter Electrode
TS – Threshold Switching
VRS - Volatile Resistive Switching

1

STATE OF THE ART

1.1 History of The Memristor

Leon Chua first proposed the concept of the memristor in 1971. According to circuit theory, four fundamental variables—current, voltage, charge, and flux—define the relationships between two-terminal circuit elements: resistors, inductors, and capacitors. The relationship between flux and charge was the only one not associated with a known circuit element. Chua hypothesized that this relationship could be represented by a new two-terminal element, which he named the memristor. This element functions as a nonlinear resistor with memory capabilities, hence the name, derived from "memory" and "resistor". [1]

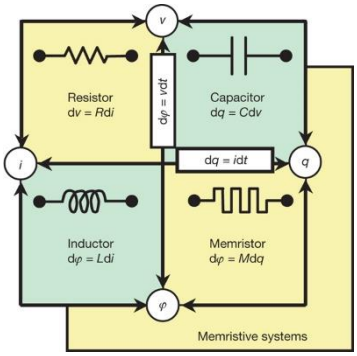

Figure 1-1 Relationship between the four fundamental circuit elements

In 1976, Chua expanded on this idea by introducing the term memristive systems, a broader class of components exhibiting memory-like behaviour. However, it wasn't until 2008 that the first memristor was physically accomplished by D.R. Williams and his team at HP Labs. Their approach involved fabricating a device consisting of a thin semiconductor layer, divided into two regions: one with high concentrations of dopants and another with minimal dopants. This structure, sandwiched between two metal contacts, allowed for the control of atomic rearrangements, which modulated the electronic current, thereby demonstrating memristive behaviour [2]

1.2 Resistive Switching Mechanism

Memristor are often classified in two common ways, the I-V characteristic, and the physical switching mechanism[3]. Considering the I-V characteristic the devices can be classified depending on the polarity of the applied current. When the set (switching from the high resistance to the low resistance state (LRS)) and reset (switching from the low resistance to the high resistance state (HRS)) processes are governed by different polarities, the device is known as bipolar. If the same polarity governs both set and reset processes, it is referred to as a unipolar. Note that the unipolar switching can normally work in both polarities, so a bipolar behaviour can be observed even in a unipolar switching device.[3], [4]

However, both in unipolar and bipolar devices, the pinched hysteresis loop is a requirement that must be present on the I-V curve. Which can present different types of behaviour, commonly identify as abrupt switching, analogue switching (which have a non-linear but more gradual change in the resistance compared to the abrupt switching) and threshold switching.

It is worth noting that the abrupt and analogue switching are non-volatile resistive switching (NVRS), and the threshold switching is volatile resistive switching (VRS).

The classification based on the physical switching mechanism are often divided by filamentary based, phase change, electronic transition and ferroelectric effects. In the filamentary range, memristors can be divided into three key mechanisms: Electrochemical Metallization (ECM), Valence Change Mechanism (VCM), and Thermochemical fuse/antifuse mechanisms, all of which are discussed in this thesis. [4]

1.2.1 Electrochemical Metallization Cell (ECM)

Electrochemical metallization (ECM) devices, also known as cation migration memristors, consist of an active electrode (AE), place on top of the switching layer (SL), such as Ag and Cu [3] due to their high diffusivity in the switching layer. An insulating layer (typically a metal oxide) that allows the diffusion of metal ions of the AE through it acting as a solid-state electrolyte, and one inert electrode that does not diffuse easily into the switching layer, such as Pt, W, Au, Ti. The operation of ECM devices relies on the formation and dissolution of a conductive filament (CF) through redox reactions and the migration of cations[5]. The selection of the AE material is critical as it differentiates between OxRAM and CBRAM.

When a positive voltage is applied to the active electrode, oxidation occurs at its interface. Metal cations are generated and migrate toward the inert counter-electrode (CE). These cations are reduced at the CE and aggregate, forming a conductive filament that spans the insulating layer, switching the device to a low-resistance state. The insulating layer allows the metal cations to move through it efficiently. Common materials for this insulating layer include HfO_2, SiO_2, Ta_2O_5, and Al_2O_3, with film thicknesses of just a few nanometres. [6]

To reset the device to a high-resistance state, a negative voltage is applied to the active electrode, initiating an electrochemical dissolution process. The metal cations drift back towards the AE, breaking the conductive filament, thus returning the device to its original state. However, the CF does not completely rupture resulting in a lower subsequent set voltage. This process is called electroforming. [5]

In Electrochemical Metallization (ECM) memristors, Joule heating plays a critical role in the reset process, particularly in the dissolution of the conductive filament. As a high current flows through the

device, Joule heating induces localized temperature increase, especially at the weakest points within the filament. This heat accelerates the electron-transfer reactions, which are enhanced near the hot spots, typically at the thinner regions of the filament, such as the top of a conical filament shown in figure 1-2e [7].

The shape of the conductive filament is a crucial factor affecting memristor device performance. Research highlights various filament configurations, including an inverted cone shape, where the CF is thicker near the counter electrode and thinner near the active electrode. This conical structure forms as metal atoms accumulate near the CE after interacting with electrons, and the filament grows toward the AE. In other cases, the CF may be thicker at the AE and thinner near the CE. These different shapes are influenced by kinetic factors such as ion mobility and redox reaction rates, which govern filament growth dynamics in the electrolyte. The weak conductive filaments in ECM [3] results in diffusive memristors with a threshold switching (TS) mechanism, that undergo a self-rupture procedure, where the relaxation time depends on the size and morphology of the CF [5]. The CFs, often composed of discontinuous nanoclusters in thin film electrolytes, exhibit diverse dynamic behaviours influenced by kinetic factors such as ion mobility and redox rates, leading to the volatile nature of the TS behaviour[6]

By controlling the formation and dissolution of these filaments, ECM devices can achieve both volatile and non-volatile switching, making them promising candidates for a variety of memory and logic applications. [5]

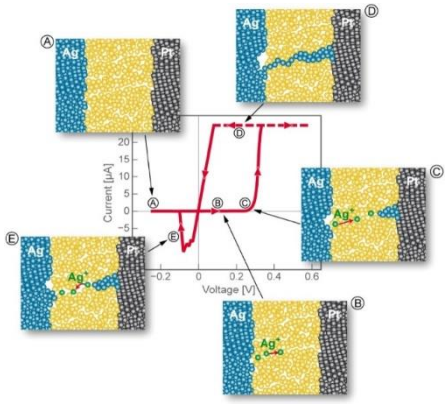

Figure 1-2 Steps for the creation of the filament and curve comparison[8]

1.2.2 Valence Change Mechanism

While there are still uncertainties about the detailed workings of the valence change mechanism, it is widely accepted that the migration of oxygen anions under an external electric field drives this process [6]. Valence Change Memristors operate based on the anion migration, particularly oxygen ions, within the oxide layer. This migration leads to the creation of oxygen vacancies, which form conductive filaments that enable the switching behaviour of the device [3]. The movement of oxygen ions induces a redox reaction that alters the valence state of the metal cations in the oxide layer, causing a stoichiometry change. [3]

Valence Change Memristors function through the migration of oxygen anions within an oxide layer, a process driven by the application of an external electric field. This migration results in the accumulation of oxygen vacancies, which create conductive filaments that enable the resistive switching

of the device[9]. The oxygen ion movement triggers redox reactions, leading to a valence change in the metal cations within the oxide. This mechanism is commonly observed in oxides such as tantalum oxide (TaO_x), hafnium oxide (HfO_x), strontium titanate (STO), and (AlO_x) [9]where the switching mechanism depends on the formation and annihilation of oxygen-deficient filaments [3], [4], [6]

During the SET process, a positive voltage causes oxygen vacancies to move toward the cathode, forming a conductive filament that shifts the device from a high-resistance state to a low-resistance state (LRS). The RESET process is initiated by applying a reverse voltage, which causes oxygen ions to migrate back and fill the vacancies, disrupting the conductive path and returning the device to its high-resistance state. [6]

Additionally, Joule heating plays a role in the switching operation, in the reset process. When a voltage pulse is applied, localized heating occurs, accelerating the migration of oxygen ions and enhancing the filament formation and dissolution process.[3]

VCM cells often require an initial forming step, which reduces the oxide layer and establishes the filamentary region for switching. Once formed, the conductive filament grows or shrinks depending on the applied voltage, controlling the switching between resistance states[7].

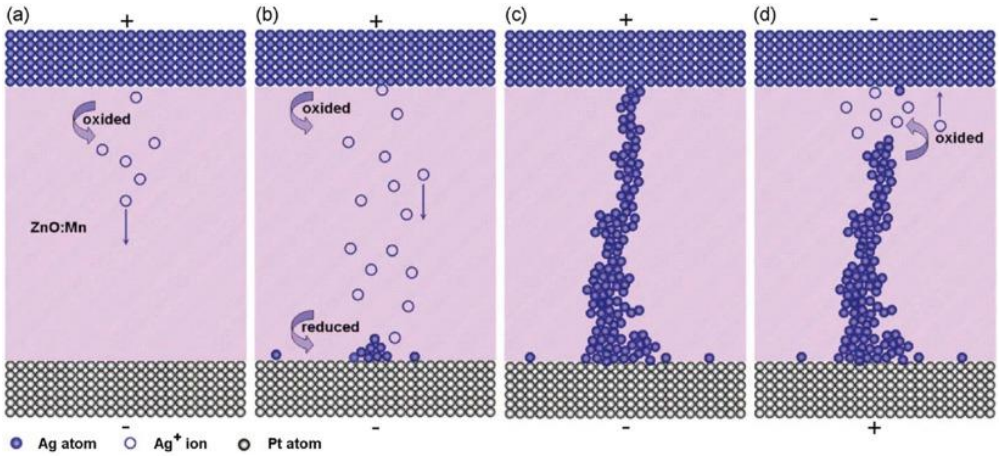

Figure 1-3 Valence change formation[6]

1.2.3 Unipolar Physical Switching Effects

In unipolar memristors, resistive switching is primarily driven by the Joule heating effect also known as fuse/anti-fuse mechanism. During the SET process, a conductive filament forms, similar to the Valence Change or ECM [3], [5] mechanism in bipolar switching devices. However, the RESET process in unipolar memristors is different because it does not depend on voltage polarity but is instead dependent on voltage amplitude. This means that after the formation of the filament, the device can be reset to a high-resistance state by applying either positive or negative voltage (figure 1-4), as long as the voltage amplitude is sufficient. The unipolar switching can happen either on the positive or negative side[4]

The key to this switching behaviour lies in Joule heating. During the reset process, the heat generated by high current flowing through the conductive filament causes the filament to rupture at its

weakest point. This heat also facilitates the recombination of oxygen ions with oxygen vacancies, disrupting the filament and increasing the device's resistance.[9]

The thermal dissolution model explains this in more detail: oxygen ions (O^{2-}) accumulate near the anode during the SET process due to a concentration gradient. Joule heating during the reset activates these oxygen ions, causing them to combine with oxygen vacancies (V_o^{2+}), which ultimately leads to the rupture of the CF and the transition to the HRS.[4], [5], [9]

The structure of this devices often includes the same inert electrode as both top and bottom, creating a symmetric architecture.[3]

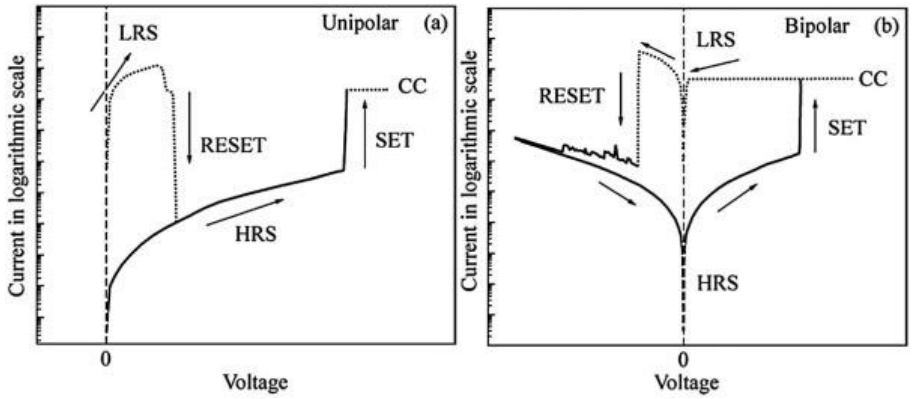

Figure 1-4 Unipolar and bipolar classic curves [4]

1.2.4 Threshold Switching

As mentioned in section 1.2.1 CBRAM devices exhibit versatile switching, and controlling the configuration of the filament can lead either to VRS, also called diffusive memristor, or NVRS[5]. The retention characteristics of the devices are closely related with the dendritic branching structures inside the switching layer often present in ECM, which can be controlled by the current compliance**.** As the applied current increases so does the number of filament branches improve the retention time. Furthermore, the thickness of the branches increases when more pulses are applied[6].

The formation of a weaker CF leads to volatile threshold switching (TS)[5]. The rupture of these filaments typically occurs through a spontaneous dissolution process driven by the interfacial energy minimization between the filament and the electrolyte matrix. This process is especially dominant in thin electrolytes, where the filament contracts rapidly under the driving forces of interfacial energy minimization[10]. It is worth noting that for low voltages the TS device will always return to the initial state[3].

Diffusive memristors, like ECM, have a threshold voltage. Once the applied voltage surpasses the threshold, the resistance of the device drops significantly, allowing current to flow freely. However, this switching is volatile, meaning the device reverts to its original HRS as soon as the voltage falls below the threshold, preventing current from flowing[3]. This volatility makes threshold memristors particularly suitable for applications like selectors in crossbar memory arrays, where temporary change in conductivity is needed. Additionally, TS helps reduce sneak currents in memory arrays, improving

both energy efficiency and the reliability of the memory system by ensuring that only selected memory cells conduct at any given time[11].

1.3 Atomic Layer Deposition

The name atomic layer deposition dates to early 2000's, before it was called atomic layer epitaxy (ALE). The reason for the change is a result from the fact that most processes do not grow epitaxially from the substrate.[12]

The advantages that the ALD provides is layer by layer deposition at relatively low temperatures and pressure making it very viable at the industry level. Because of his self-limiting nature, derived by the sequential addition of precursors the results are thin film with high conformality, morphology and control over the thickness. [13]

The ALD deposition starts with the occupation of the active sites present in the surface of the sample through adsorption of the first precursor released in the vacuum chamber. This process occurs until the surface reaches saturation, therefore the self-limiting process. This saturation point is temperature dependent however most ALD cycles have a temperature window at which the deposition rate is constant. To be considered a true ALD deposition one single monolayer needs to be deposited.

After the first precursor reaches it saturation there is the purge time, with the intention to clean the chamber for the second semi-cycle. In the second semi-cycle another precursor is released in the vacuum chamber until it reaches the saturation point, and consequently be purged, and the end of the cycle is achieved. [13]

The atomic layer deposition (ALD) of Al_2O_3 typically involves two main precursors: trimethylaluminum (TMA) [$Al(CH_3)_3$] and water (H_2O). This process proceeds through two alternating half-reactions.

The first half-reaction begins with the introduction of the precursor (in this case TMA) into the reactor where it reacts with hydroxyl (-OH) groups on the surface of the substrate. Once all available hydroxyl groups have reacted, the process stops. The chemical reaction can be written as:

$$-OH+Al(CH_3)_3 \rightarrow -O-Al(CH_3)+ CH$$

Here, methane (CH_4) is released as a byproduct, and the surface becomes terminated by $-CH_3$ groups.

The second half-reaction: starts after the purge of the CH_4 byproduct with the release of water vapor, that will react with the $-CH_3$ groups to regenerate the -OH surface, preparing it for the next TMA exposure. This reaction also releases methane as a byproduct:

$$Al(CH_3)+H_2O \rightarrow -AlOH+CH_4$$

This half-cycle stops once all the $-CH_3$ groups have reacted, regenerating a hydroxyl-terminated surface, allowing for the next TMA half-cycle to begin.

This alternating process leads to the precise deposition of Al_2O_3 films in a layer-by-layer fashion[14]

1.4 Aluminium Oxide Switching Layer By ALD

The potential of Al_2O_3-based materials for use in electronic synapses has been demonstrated in several experiments, confirming their viability for memristor-based applications. However, the

development of more sophisticated Al_2O_3-based memristors as artificial synapses is still in its early stages, with limited reports available. This gap highlights the need for further exploration and experimental verification of different Al_2O_3 structures in neuromorphic devices.[9]

Recently, AlO_x (a sub-stoichiometric form of Al_2O_3) has gather attention in resistive random-access memory (RRAM) materials due to its favourable properties, including a large band gap (~9 eV) and low RESET current (~1 μA). AlO_x can be used either alone or in stacked configurations with other RRAM materials to enhance the reliability and reproducibility of device characteristics.[9]

The limited availability of reports on Al_2O_3-based memristors for synaptic applications could be attributed to the fact that Al_2O_3 alone does not always exhibit the desired switching uniformity or performance for advanced neuromorphic applications.[15]

Based on the position and stoichiometry of the aluminium oxide layer, it can have opposite purposes[3]. The insertion of a thin Al_2O_3 layer between the bottom electrode and the switching layer extremely improves the switching characteristics and uniformity increasing control over the filament position. The Al_2O_3 layer, due to dense dielectric properties and good thermal characteristics, can shift the filament rupture away from the bottom electrode increasing the insulating gap[16]. The Al_2O_3 layer controls the filament formation by, acting as a O interstitial former making the creation of oxygen vacancies difficult for VCM devices[17]. For ECM devices, when combined with a fast ion conductor[18] or a high-level defect layer that can create a stationary filament[19], will help the formation/dissolution of the filaments under an external electric field, with a slower rate preventing the rapid and uncontrolled filament grow due to low ion mobility. On the other hand, the utilization of AlO_x between the top contact and more stable switching layer, increases the number of defects present on the switching layer creating more easily a conductive filament. [20], [21]

The top contact plays a crucial role in determining the resistive switching (RS) mechanism and overall performance of Al_2O_3-based memristor devices. In devices like Au/Al_2O_3/ZnO/FTO and Ag/Al_2O_3/ZnO/FTO, the reactivity and material properties of the top electrode significantly influence the physical switching behaviour and conduction mechanism. The difference in reactivity between gold (Au) and silver (Ag) electrodes leads to distinct RS mechanisms in these devices.[22], [23]

In the Au/Al_2O_3/ZnO/FTO device, the switching occurs at the Al_2O_3 layer, with the ZnO layer serving as a source of oxygen vacancies, which contribute to the switching process. The Au top electrode does not directly participate in the formation of conductive filaments, resulting in a self-limited bipolar behaviour with abrupt SET and gradual RESET processes. On the other hand, in the Ag/Al_2O_3/ZnO/FTO device, the more reactive Ag electrode introduces metal cations into the switching mechanism, leading to a different RS process where metal ions play a key role.[22], [23]

Additionally, factors such as roughness of the electrode surface, that influences the filament formation, and current compliance play a significant role in controlling the switching dynamics. Limiting current during filament formation reduces variability in the LRS, while higher reset currents ensure the proper rupture of filaments, preventing device degradation over repeated cycles.[24]

2

METHODS AND MATERIALS

2.1 Device Fabrication

2.1.1 Substrate Preparation

To eliminate impurities from the Corning glass substrates, a thorough cleaning process was carried out. First, the substrates were immersed in an acetone solution and subjected to ultrasonic cleaning for 10 minutes at 40°C. They were then transferred to an isopropyl alcohol (IPA) solution and again treated with ultrasound for another 10 minutes. Following this, the substrates were rinsed with deionized water and placed on a heating plate at 120°C for 10 minutes. This cleaning procedure was consistently performed on every substrate used in this thesis prior to the deposition of the bottom electrode.

2.1.2 Bottom Contact

Initially 86 nm of AZO was experimented as bottom electrode. The deposition followed 4 ALD super cycle, at 150ºC with Dez, TMA and H2O as precursors. The super cycle was divided in 1 Al_2O_3 cycle of TMA and H_2O with pulse/purge respectively of 0.15s/5s/0.5s/4s and 101 ZnO cycles with Dez and H2O with pulse/purge times respectively of 0.5s/8s/3s/4s. An attempt with Mo by RF sputtering was implemented. In the sputtering technique the substrates inside the chamber form a coating from the solid material being bombarded with gas particles that gain kinetic energy and adhere to the surface of the sample. The deposition was carried out at room temperature, with a flow rate of 50 $sccm$ of Argon, an RF power of 175W and a deposition pressure of 1.7 $mTorr$. Finally, by e-beam, a 20 nm layer of Pt as bottom contact was deposited, for a better adhesion a 20 nm Ti layer had to be previously applied. The process consists of evaporations of the solid material by applications of charged electrons throw a magnetic field inside the vacuum chamber. For the AZO and Mo samples the entire substrate was covered by the bottom contact without any patterning, unlike the Pt/Ti which will be later explained.

2.1.3 Switching Layer

The Al_2O_3 switching layer, was deposited by ALD over the bottom contact, with a thickness of 5 or 10 nm, for the AZO devices, and 5 nm for the Mo and Ti/Pt samples. The recipe followed for the Al_2O_3 layer was the same for every sample, changing only the number of cycles depending on the thickness desired. For the Al_2O_3 layers deposition the ALD at 150 °C, involving 51 (5nm) and 95 (10nm)

cycles of trimethylaluminum (TMA) and H_2O, with pulse/purge step durations of 0.15s/10s (TMA) and 0.075s/10s (water)

Additionally, to the fabrication of the previous devices, on the substrate with the pattern Ti/Pt as bottom contact, other alternatives were conducted. A single 6 nm thick non-stoichiometric layer of AlO_x was applied on the substrates with two different temperatures, 150ºC and 300ºC, while the H_2O precursor time was 0.025 s for both samples. The application of a bilayer with 5nm Al_2O_3 and on top a 6nm layer with AlO_x to improve the performance was attempted. The Al_2O_3 layer used followed the same recipes mentioned earlier.

2.1.4 Top Contact

For the devices with AZO, the top contact depositions were initially made by e-beam with different materials, such as, Al, Ti/Au, Ti/Ag, Ag, with a thickness of 100 nm, 6 nm/60 nm, 6 nm/60 nm, 100 nm respectively. A mechanical mask with 100 μm of diameter was taped on top of the switching layer using kaptan.

To enhance device performance, a plasma treatment was applied to the switching layer moments before the deposition of the copper via RF sputtering. This treatment was performed on devices with Mo, and AZO as bottom electrodes. The RF power of the Cu target was of 50W for the three different plasma exposure durations of: 0 minutes, 10 minutes, and 20 minutes with a substrate bias of 10W and a flowrate of 20 $sccm$ of argon. Following the plasma treatment, mechanical masks were placed over the switching layer to facilitate the deposition of a 150 nm Cu layer by sputtering at room temperature, with a flow rate of 20 $sccm$ of Argon, an RF power of 150W and a deposition pressure of 1.7 $mTorr$. In the final structure, a 100 nm Cu top electrode was deposited using e-beam evaporation, since there was no need for the argon plasma treatment.

2.1.5 Fully patterned devices

The devices consisting of Ti/Pt as bottom electrode suffered a lift off process. This began with the application of a negative photoresist onto the Corning glass substrate via spin coating. Photoresists come in two types: negative and positive. Negative photoresist is soluble in the developer unless exposed to UV light, which hardens it. After applying the photoresist layer, the sample is aligned with a patterned mask using a mask aligner and subsequently exposed to UV light. The exposed areas become insoluble, while the unexposed areas remain soluble. The sample is then immersed in a developer solution to reveal the pattern in the areas exposed to UV light. Following this, the bottom electrode material is deposited across the entire sample. Finally, the lift-off process is completed by cleaning the sample with acetone and alcohol, which removes the photoresist, and any material deposited on top of it leaving only the patterned bottom electrode defined by the mask. For these devices the switching layer was deposited across the entire sample without the lift off process. The deposition of the top contact followed the same process as the bottom contact.

In the following table, there is a depiction of every method and parameter as well as structure used in the device fabrication.

Table 2-1 Summary of the device fabrication and structure

Top Contact	Al; Ti/Au; Ti/Ag; Ag	Cu	Cu	Cu (pattern)
Argon plasma treatment	--------	0 min, 10 min, 20 min	0 min, 10 min, 20 min	---------
Switching layer	Al_2O_3	Al_2O_3	Al_2O_3	AlO_x / Al_2O_3 (pattern)
Temperature deposition	150 ºC	150 ºC	150 ºC	150 ºC or 300 ºC / 300 ºC
Thickness	5 and 10	5 nm	5 nm	5 nm / 5 nm
Bottom Electrode	AZO	Mo	AZO	Ti/Pt (pattern)

2.2 Electrical And Chemical Characterization

The electrical characterization of the devices was carried out using a Keithley 4200SCS semiconductor characterization system in combination with a Janis ST-500 cryogenic probe station. The device connections were adjusted based on the specific test being performed. For direct current (DC) measurements, the devices were connected to two Source Measurement Units (SMUs). In all experiments, input signals were applied to the top electrode while the bottom electrode was grounded.

X-ray photoelectron spectroscopy (XPS) measurements were performed using a Kratos AXIS Supra instrument equipped with a monochromatic Al Kα radiation source. The X-ray power was set to 150 W, and a pass energy of 10 eV. The fitting procedure was conducted with two components with identical full width at half maximum and a fixed energy separation.

3

RESULTS AND DISCUSSION

This chapter is structured into three sections. The first two sections will analyse the outcomes of the initial experiments, providing a thorough examination of the factors that contributed to the device's underperformance. These sections will investigate the challenges encountered with different electrode materials, and the inconsistent behaviour observed during pristine and IV tests. By understanding the results obtained from the first two attempts an innovative approach is explained in the third section, which focus on the adjustments made to the device structure and fabrication process. The last section will explain the logic behind the introduction of an AlO_x defective layer, material and structure optimization to improve device performance.

3.1 AZO/ Al_2O_3

Based on research previously done at CENIMAT which concluded that the more time passed between the deposition of the bottom contact and the switching layer the less uniform was the behaviour of the devices in the same sample, an AZO bottom contact was selected combined with the Al_2O_3 switching layer deposited by ALD. In this case the deposition of the bottom contact and switching layer was completed without removing the sample from vacuum.

The top contact materials of the devices were experimentally varied, with aluminium (Al), silver (Ag), and gold (Au) being tested. Each material exhibited distinct electrical behaviour. The following subchapter will discuss the electrical characterization of these variations in detail.

The first test conducted on the devices is the pristine test, which provides a general idea of the device's behaviour. By applying a forced voltage between -1 and 1 V in dual-sweeping mode, we can analyse the device's response. Figures 1 (a) and (b) display the average curves for each device. This allows us to confirm that the thickness of the switching layer significantly impacts device performance, particularly in devices with TiAg and Ag top contacts, which exhibited the most variation. Furthermore, using Ti at the interface to the Al_2O_3 increases the conductivity of the device.

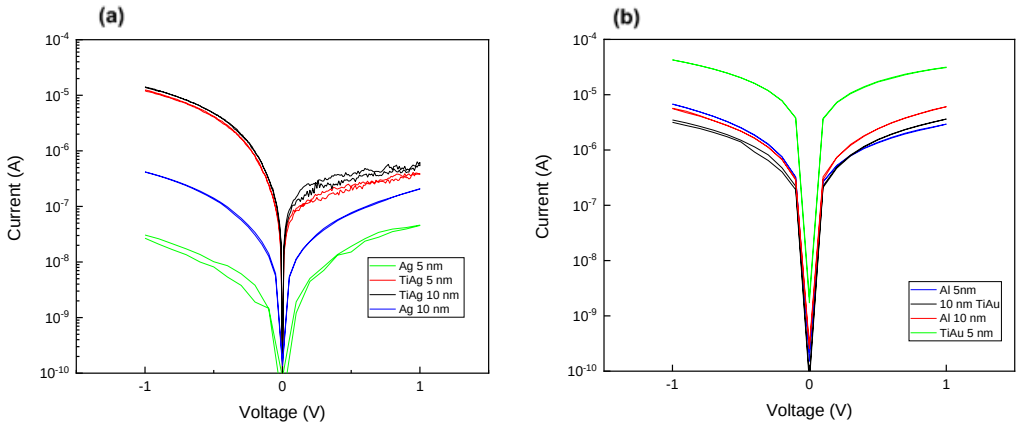

Figure 3-1 **(a)**Pristine curves for devices with Ag and TiAg as top contact, with 5 and 10 nm switching layer thickness **(b)** Pristine curves for devices with Al and TiAu as top contact, with 5 and 10 nm switching layer thickness

Although the rectification is not a requirement in memristor devices while performing the pristine, in this first scenario represents a key indicator of whether the devices would exhibit any switching characteristics. The rectification process can be attributed to several factors, including varying conduction mechanisms at the interface and an asymmetric structure, which creates different work functions. Non-linear ion migration, such as oxygen vacancies or metal ions, tends to drift more easily in one direction due to mechanisms like Schottky or Poole-Frenkel conduction. In figure 3-1 (a), a slight rectification could only be observed for the Ti/Ag electrodes. Potentially, this could indicate an increased oxygen-deficiency at the top electrode interface, which would facilitate electron injection over this interface.

The Al_2O_3 based memristors devices can operate as ECM or VCM, depending on the electrodes or the architecture. The ECM behaviour requires an active electrode and an inert counter electrode, so the devices with the Ag as top electrode should present this type of physical mechanism. On the other hand, devices with Al or Au should present VCM type of behaviour. In a situation of an oxygen-deficient top interface region (i.e. more positively charged oxygen vacancies), to ensure the device operates as expected, the set process should occur on the positive side and the reset on the negative, according to the filamentary VCM. The lack of asymmetry in the device architecture, due to the use of AZO (an inert electrode) paired either with Al or Au, both inert electrodes could result in the lack of memristive behaviour.

Both the Al and Ti/Au configurations, with 5 nm and 10 nm thickness, presented linear behaviour and lack of rectification, thus no further curves will be displayed for these devices figure 3-1 (b).

3.1.1 TiAu And Al Top Contact

Studies indicate that Al_2O_3 memristors face difficulties in forming oxygen vacancies[17]. Combined with the lack of defects typically presented by ALD deposition means that switching characteristics for VCM type of devices are difficult to obtain. This results in the linear behaviour present on the pristine curves in figure 3-1 (b).

One of the main challenges with the Al device arises from the interface between the AZO bottom electrode and the Al_2O_3/Al top contact structure. While both Al [24] and AZO[25] are commonly used as electrodes, their combination in this configuration results in a symmetrical defect profile [5]. Research suggests that ohmic conduction dominates at low electric fields in the Al/Al_2O_3[26] structure, and a similar mechanism is likely at play at the AZO/Al_2O_3 interface.[27] However, the presence of at least one non-linear conduction mechanism is essential for memristive switching in metal/oxide/metal systems[28].

The nonlinear behaviour that is can be observed in figure 3-1 (a), can be limited by the electrode or the switching material. In this case the change from Al to Au device eliminated the symmetric conduction mechanism by inserting on the top electrode a pool-frankiel emission. [29], but, a similar behaviour can still be observed, caused by the Al_2O_3, that acts as an oxygen vacancy barrier, preventing filament formation[17].

3.1.2 TiAg And Ag Top Contacts

After the pristine test is finished each device is swept with increasingly higher voltage to find the exact voltage for the electroforming, which is the activation process of the cell. Since Al_2O_3 cells have a filamentary switching mechanism, an electroforming process is required before SET and RESET curves can be obtained.

In order to perform the forming step, the bottom contact is grounded, and current is applied in dual sweeping mode to the top contact. Since the active electrode, in this case the Ag or the Ti/Ag, is deposit on top of the switching layer the forming process is perform on the positive side. In the figures 3-2 (a) and (b) and 3-3 (a) and (b), we can see a typical curve obtained with the Ag top contacts with and without the Ti adhesion layer.

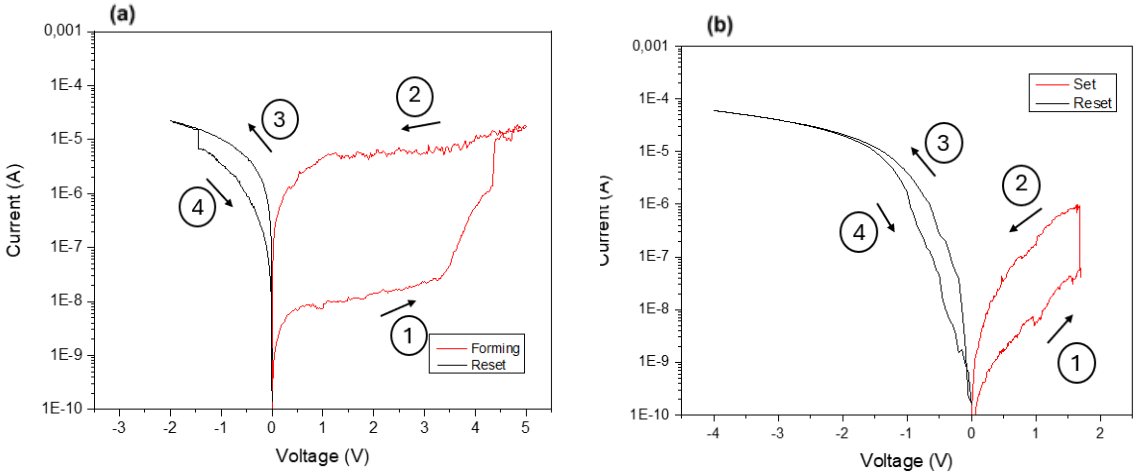

Figure 3-2 (a) Switching characteristics typical behavior of AZO/ Al_2O_3 (10 nm) /TiAg (b) Switching characteristics typical behavior of AZO/ Al_2O_3 (10 nm) /Ag

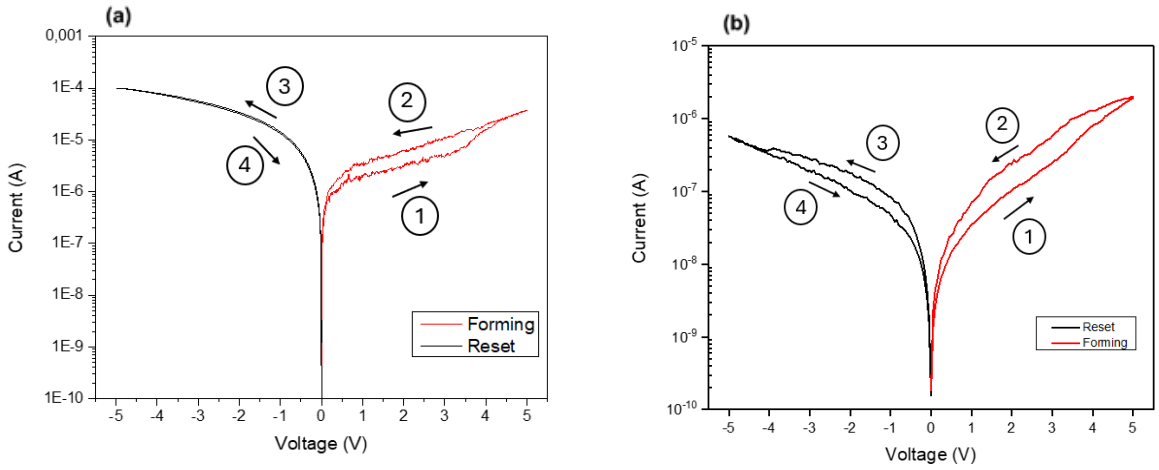

Figure 3-3 **(a)** Switching characteristics typical behavior of AZO/Al2O3 (5 nm) /TiAg **(b)** Switching characteristics typical behavior of AZO/Al2O3 (5 nm) /Ag

The ability of the Ti adhesion layer to increase the oxygen vacancies is confirmed by comparing figures 3-2 (a) and (b). The higher voltage required to operate forming and the abrupt switching in the TiAg sample indicates a thicker insulator layer with more defects. The interaction between the titanium and the Al_2O_3 produces TiO_2, that acts as an oxygen absorber, enhancing the formation and stability of the conductive filament (table 3-1).[17], [30]. Furthermore, the devices with the 5 nm Al_2O_3 layer did not result in stable forming, however in figure 3-2 (b) more trapping occur when compared to figure 3-3 (b).

Although the improvement from the previous tests some problems remain. As we can see even after the forming is obtained the device could performed reset, due to a low ion mobility and the creation of a strong filament caused by high forming voltage[20], the rupture did not occur.

3.2 Al_2O_3 With Argon Plasma Treatment

Based on the information gathered from the previous section, some alterations to the device architecture and treatment were made.

The use of Cu in memristor devices, instead of Ag, is well study. Both Cu and Ag are categorized as electrochemically active electrodes, meaning they participate in critical oxidation-reduction reactions that facilitate the formation of conductive filaments. However, the slower mobility of Cu can lead to more controlled filament growth, potentially enhancing trapping efficiency and overall device stability.[31].

To further enhance device performance, increasing the concentration of defects is necessary[17] seen with the Ti layer in the previous chapter. Another method for achieving this goal is through argon plasma treatment, which is applied to the switching layer to encourage the formation of more defects[32]. This process enhances the density of vacancies, particularly important in devices using Al_2O_3 as part of the switching stack, contributing to better control of the switching mechanisms and improving overall performance,.[19]

To cause some defects on the switching layer, different times of argon plasma treatment were applied to the Al_2O_3 surface in situ prior to the top contact deposition. Furthermore, a high series resistance was suspected from the IV curves obtained with the AZO bottom contact (the current never surpassed 0.1 mA). Due to the limited conductivity of AZO compared to a metal, Mo was also tested as alternative bottom electrode[33]

3.2.1 AZO/ Al_2O_3/Cu

The pristine curves of different devices with 0, 10 and 20 minutes of argon plasma treatment are shown in fig. 3-5 (b). Two very distinct behaviours can be seen clearly in each fig. 3-4 (a) and (b), and 3-5 (a), a highly conductive behaviour, caused by the pressure ensured by the tip of the probe station on the sample and a lower one that shows the device behaviour. The increase conductivity of the pristine could be explained by an improved electrical contact between the tip and the sample, however the difference would not be as severe, or the increased pressure caused a contact resistance reduction, resulting in a deformation of the surface asperities, enhancing local conduction pathways. This improved interface facilitates the formation of conductive filaments and local electric fields, which are crucial for the resistive-switching behaviour of the device.[34] However the negative influence of the pressure on this device will be better explain in subchapter 3.2.1.

Comparing the curves with high conductivity with the ones with low conductivity, we see the presence of noise in the latter. This happens because of a possible bad contact between the tip of the probe station and the sample, since this behaviour is present in every figure, especially with 0 min of plasma treatment that has lower current.

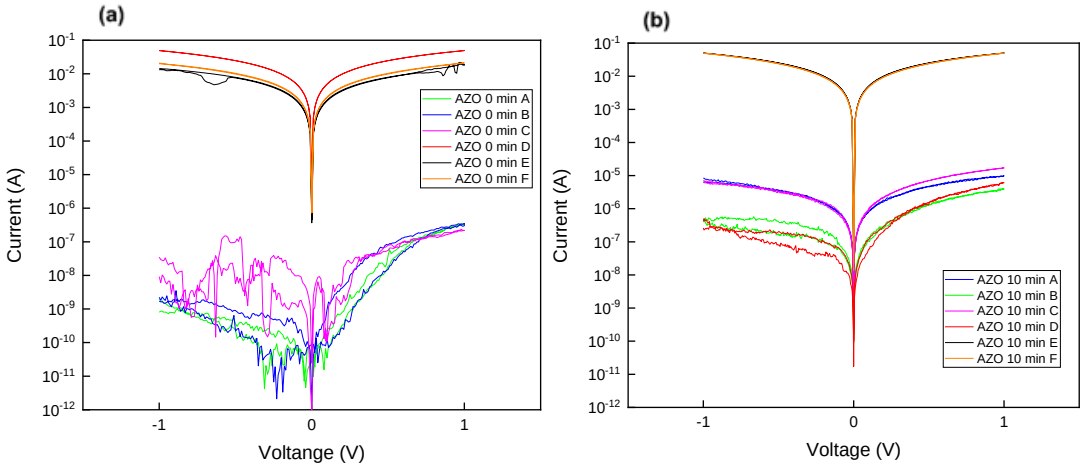

Figure 3-4 **(a)** Pristine state of different AZO/Al_2O_3/Cu with 0 min of Argon plasma treatment devices **(b)** Pristine state of different AZO/Al_2O_3/Cu with 10 min of Argon plasma treatment devices

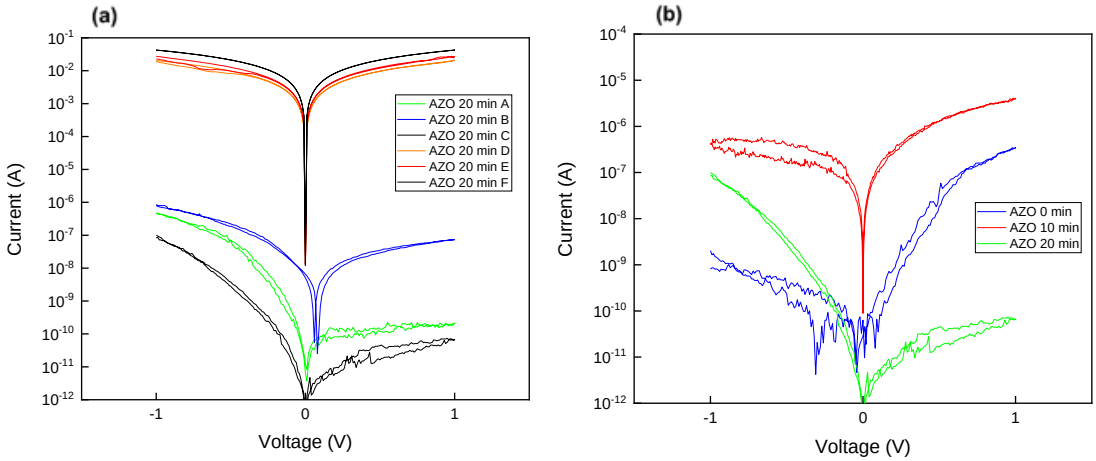

Figure 3-5 **(a)** Pristine state of different AZO/Al2O3/Cu with 20 min of Argon plasma treatment devices **(b)** Pristine of the three different times tested on the AZO/Al_2O_3/Cu samples

The I-V characteristics of the pristine sample, subjected to varying durations of argon plasma treatment, reveal significant changes in its electrical behaviour. As the time of the plasma treatment increased from 0 to 20 minutes, the rectification shifts from a negative bias (0 minutes) to a positive bias (20 minutes), indicating a modification of the diode-like properties. Argon plasma treatment introduces additional surface defects, particularly oxygen vacancies, which act as charge-trapping centres, enhancing filament formation and charge transport across the device. This modification of the defect profile is responsible for the observed increase in conductivity and the shift in rectification behaviour, as increased defects reduce the barriers for electron injection and alter the symmetry of the current flow.[35]

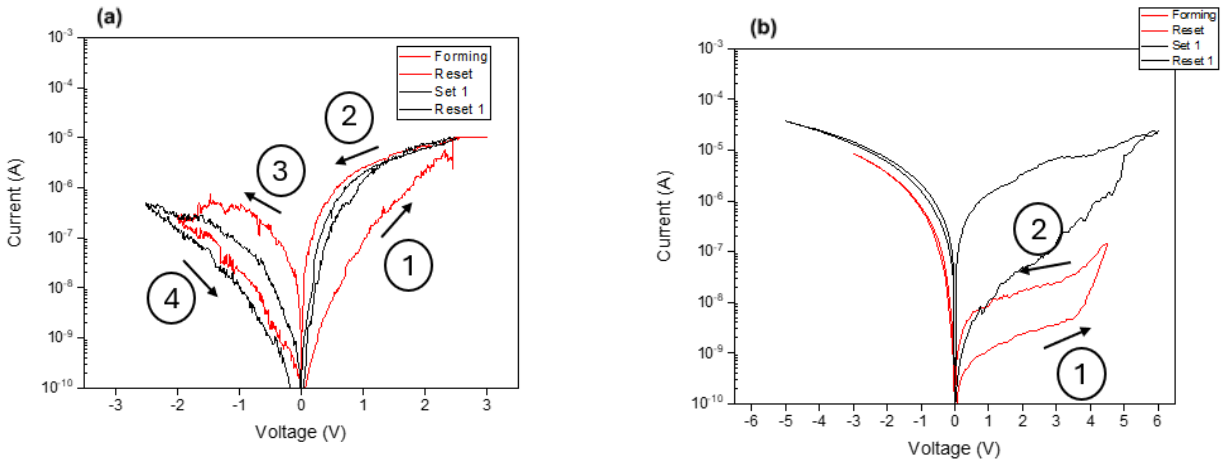

Figure 3-6 **(a)** Switching characteristic of AZO/Al2O3/Cu with 0 minutes of argon plasma treatment **(b)** Switching characteristic of AZO/Al2O3/Cu with 10 minutes of argon plasma treatment

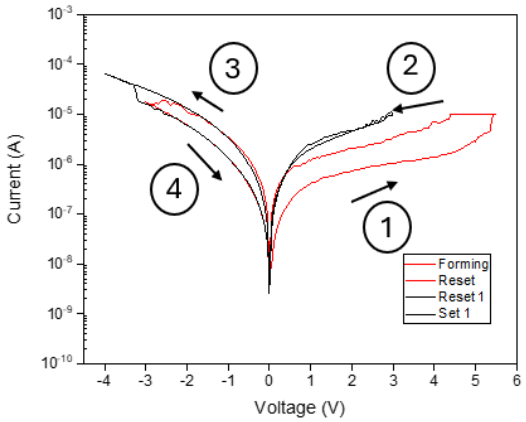

Figure 3-7 Switching characteristic of AZO/Al2O3/Cu
with 20 minutes of argon plasma treatment

The figures above prove the fact that the argon plasma treatment did in fact create irregularities in the Al_2O_3 matrix. The lack of the reset process after the forming with fig 3-6 (a) and (b) is caused by the thin layer of Al_2O_3, (5 nm). The layer is too thin so the plasma treatment introduced too many defects that could have gradually improved the mobility of the Cu ions. The devices create a strong filament due to the presence of the extra vacancies[20]. Rupturing the CFs becomes challenging even when a high negative voltage is applied. Figure 3-7 is a perfect example, since the reset attempt is performed with high voltage -4 V, resulting in a small change in conductance. The consequent set has inherent high conductivity and does not produce a significant switch because the gap between the broken filament is extremely narrow, and it is easily formed when a positive voltage is applied.

The idea behind the Al_2O_3 thickness reduction was to obtain a lower forming voltage, which had a positive effect in the sample with 0 min of argon plasma treatment, resulting in a 2.2V forming voltage when compared to the devices of figures table 3-1. The analogue switching present in figure 3-6 (a) could also be caused by trapping of Cu that have slower mobility then Ag.

3.2.2 Mo/ Al_2O_3/Cu

In figures 3-8 (a) and (b), 3-9 there is a depiction of the pristine curves for the different argon plasmas treatments for the Mo/Al_2O_3/Cu structure. The times for in situ plasma treatment on the Al_2O_3 film prior to Cu deposition were 0, 10 and 20 minutes.

The initial behaviour showed by the samples with 0 and 10 min (figure 3-8 (a) and (b)) and the presence of two highly conductive electrodes leads us to believe of a problem with the Mo contact. However, other studies with similar device configuration demonstrated lower current[36], which shifts the focus to the insulator thickness. A thinner insulator layer has weaker dielectric strength, making the device susceptible to a break down, therefore conducive.

.

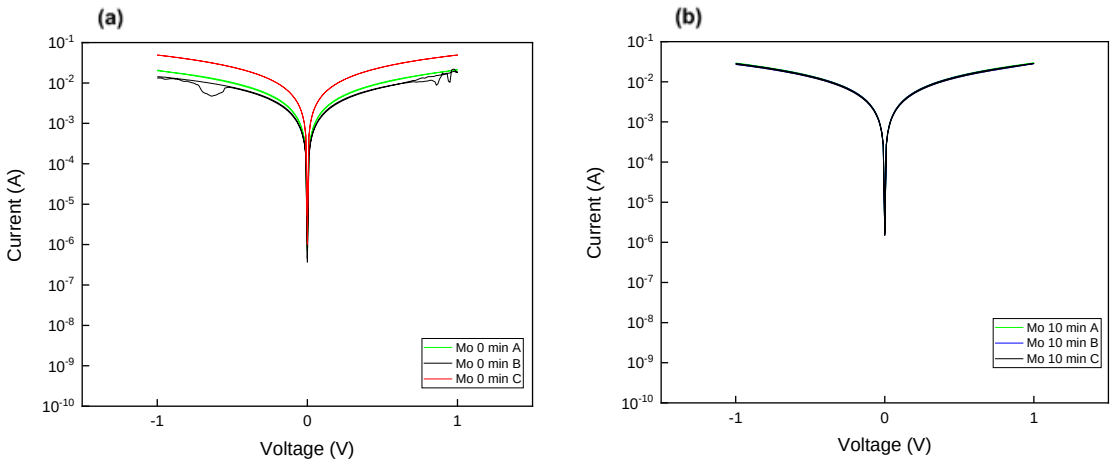

Figure 3-8 **(a)** Pristine state of three different devices from the Mo/Al_2O_3/Cu sample with 0 minutes of argon plasma treatment **(b)** Pristine state of three different devices from the Mo/Al_2O_3/Cu sample with 10 minutes of argon plasma treatment

Although the Mo samples exhibit high conductivity[36], sensitivity during electrical characterization, where the pressure applied by the probe station's tip significantly affected the measurement results, could have further increased the current values of the devices. This high-pressure sensitivity became evident as the conductivity remained largely unchanged despite increasing durations of argon plasma treatment. The underlying issue is that the pressure applied by the probe tip during electrical measurements directly influenced the device's behaviour, as seen in the pristine graph of figure 3-9. The variation in applied pressure during contact with the sample led to inconsistent results, highlighting the device's susceptibility to mechanical stress during testing.

This issue is further reinforced by comparing the two different structures with AZO and Mo, confirming that the pressure sensitivity of the samples must be carefully managed to ensure accurate characterization.

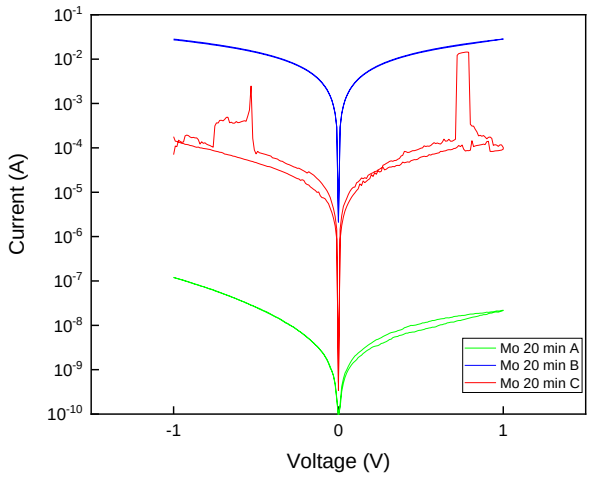

Figure 3-9 Pristine state of three different devices from the Mo/Al_2O_3/Cu sample with 20 minutes of argon plasma treatment

Either RF sputtering and ALD are deposition techniques with high uniformity[37], [38], so there are not significant thickness differences between devices, which lead us to conclude that the difference between the conductivity present in figure 3-9 did not originated from a difference in the thickness or uniformity but more likely from a pressure problem.

To mitigate the problems presented in this subchapter, patterning process was done to reduce pressure sensitivity as well as the area that can significantly alter the capacitance and the conduction mechanism. The introduction of an extra defective layer of AlO_x above the Al_2O_3 layer, to create more defects while increasing the thickness of the switching layer maintaining homogeneous the defects in the matrix.

Table 3-1 Comparison of the results from the first two batches

Device Configuration	Vset (V)	Vreset (V)	I-LRS (A)	Vforming (V)	Pristine Range
AZO/Al_2O_3 (10 nm) /Ag	----	----	10^{-5}	2.2	[-1;1]
AZO/Al_2O_3 (10 nm) /TiAg	----	----	10^{-6}	4.2	[-1;1]
AZO/Al_2O_3 (5 nm) /Cu (0 min Plasma)	2.2	-2.5	10^{-4}	2.5	[-1;1]
AZO/Al_2O_3 (5 nm) /Cu (10 min Plasma)	6	----	10^{-5}	4.5	[-1;1]
AZO/Al_2O_3 (5 nm) /Cu (20 min Plasma)	----	----	10^{-6}	5.5	[-1;1]

3.3 Defective AlO_x and bilayers

The bottom electrode chosen was platinum which the patterning process is already optimized. The limited conductivity of AZO would add too high series resistance in the case of a patterned device[33]. Two switching layer architectural structures were fabricated, a double layer made up by a more defective AlO_x matrix to induce trapping on top of the Al_2O_3, and a single AlO_x device was in order to study the importance of the Al_2O_3 in the stabilization of the conductive filament for memristive devices.

3.3.1 X-ray Photoelectron Spectroscopy

In order to understand the dominant defect involved in the resistive switching of defective Al_2O_3 by ALD, X-ray photoelectron spectroscopy was performed on the two AlO_x films produced at different temperatures as well as the standard Al_2O_3 layer. The atomic concentrations are presented in Table 3-1

and the O 1s emission are shown in Figure 3-10. The Al 2p emissions are not shown because they exhibit identical line shapes and binding energies, indicating that the films are similar in chemical state. This suggests that there is no significant difference in the bonding or oxidation state of the aluminium atoms across the films. Therefore, the factors influencing the resistive switching behaviour are more likely related to the oxygen vacancies, hydroxyl group content, and potentially the carbon content. The fitting of the O 1s emissions was done with two components of identical full width at half maximum and fixed energy separation. The O 1s component at higher binding energy represents the Al-O lattice bonds, while the lower binding energy component can be assigned to hydroxyl groups. Figure 3-10 (a) shows an Al_2O_3 film grown with the standard process. The AlO_x film grown at 300C in Figure 3-10 (b) reveals an increased amount of hydroxyl groups. This amount is further increased with a lower growth temperature of AlO_x, Figure 3-10 (c)The amount of hydroxyl groups from the O 1s emission is most likely related to the carbon content, since this also increases as the aluminium process becomes oxygen deficient and towards lower temperatures (see table 3-2). This allows us to speculate that more and more TMA precursors remain in the films.

All films are oxygen-poor, the more oxygen-poor being the supposed stoichiometric Al_2O_3 film. Comparing the AlO_x at different temperatures, a slightly more pronounced oxygen deficiency can be observed, compared to the AlO_x layer at 300C.

In light of the electrical switching results, the oxygen-deficiency cannot explain the increased defect concentration in the ALD films, since the most stable Al_2O_3 is actually more oxygen-deficient than the AlO_x layers. There are studies that indicate that Al_2O_3 introduces oxygen vacancies[15], while improving switching behaviour, by limiting the random formation of conductive filaments (CFs)[16] due to a better control over the distribution and behaviour of these vacancies [40]. However, the lower binding energy component of O1s is often misinterpreted as oxygen vacancy signal, which is impossible for a surface that has been exposed to ambient air and is consequently saturated by hydrocarbons and adsorbed water[41].

Instead of considering an increased oxygen-deficiency as the main cause for a more defective film, the amount of OH group is in fact significantly increased in layers that show more stable switching (AlO_x) (figure 3-10) and are thus more defective. As a consequence, it is concluded that the OH groups (most likely related with unreacted precursor and as such linked to carbon) are the most relevant defects responsible, which facilitate the resistive switching.[20]

Table 3-2 Calculations of the ratio of oxygen (bonded to aluminium) over aluminium, based on the atomic concentration of Al, C, and O as well as the O 1s fitting results

	Atomic Concentration [%]					
Sample	Al 2p	C 1s	O 1s	O 1s Al-O	O 1s O-H	O(Al-O)/Al
AlO_x 150ºC	30.03	17.77	52.2	36.32	15.88	1.21
AlO_x 300ºC	31.49	16.51	52	40.27	11.73	1.28
Al_2O_3	37.33	9.86	52.8	41.83	10.97	1.12

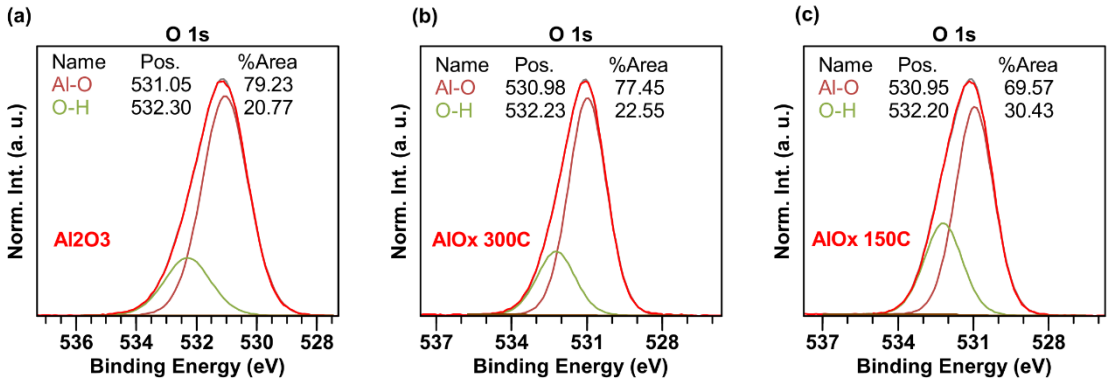

Figure 3-10 (a) shows an Al2O3 film grown with the standard process. The AlOx film grown at 300C in (b) reveals an increased amount of hydroxyl groups. This amount is further increased with a lower growth temperature of AlOx, Figure (c). The O 1s component at high

3.3.2 Pt/ AlO_x (150ºC/300ºC) Cu

A single layer of AlO_x deposited by ALD with different temperatures was assessed. However, it failed to produce results. As we can see in the fig. 3-11 the high conductivity when the pristine test is performed shows the impossibility to use this structure as a viable memristive device. This behaviour can be the result of a thin layer (only 5 nm) facilitating tunnelling and the device break [8], [26].

Since the pristine curves presented a high level of conductivity no more curves will be shown. This results however confirms the need for a more stable switching layer. A combination of two switching layers, a more defective one to work as defect doner (AlO_x) and a more stable (Al_2O_3) to prevent degradation and to improve the isolation between the electrodes[20].

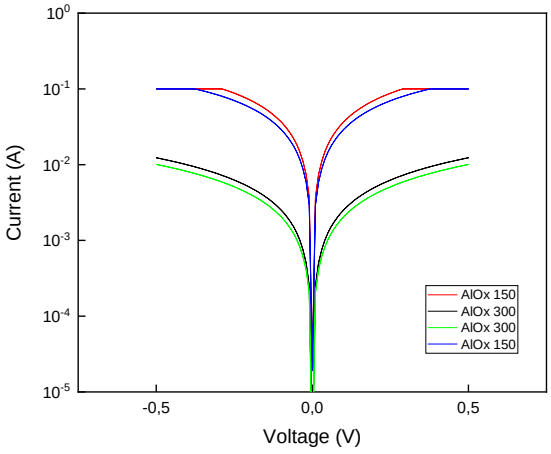

Figure 3-11 Pristine state of the TiPt/AlOx /Cu with the two different temperature depositions of the AlOx layer, 150ºC and 300ºC

3.3.3 Pt/ Al_2O_3 AlO_x (300ºC) /Cu

Since the reduction of the area and change in bottom electrode the range of the pristine test was altered to -0.5,0.5 V. The figure below shows break down on the devices 4_7, 4_8, 4_9 (the first number is the row and the second the column where the devices are located inside the sample) tested with higher voltage. The variability in the pristine state of devices arises from differences in their initial conditions, with some exhibiting pre-existing conductive filaments. This is attributed to the non-stoichiometric AlOx layer causing uneven oxygen distribution, leading to localized oxygen vacancies and intrinsic LRS or HRS states, however this will be better explained.

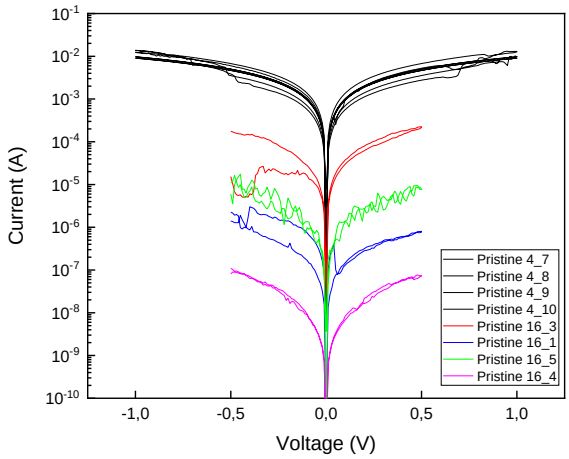

Figure 3-12 Pristine map of TiPt/$Al_2O_3AlO_x$ /Cu sample with 30 um^2 area. The AlO_x deposition at 300ºC, with two different range of voltage, -0.5;0.5 and -1;1

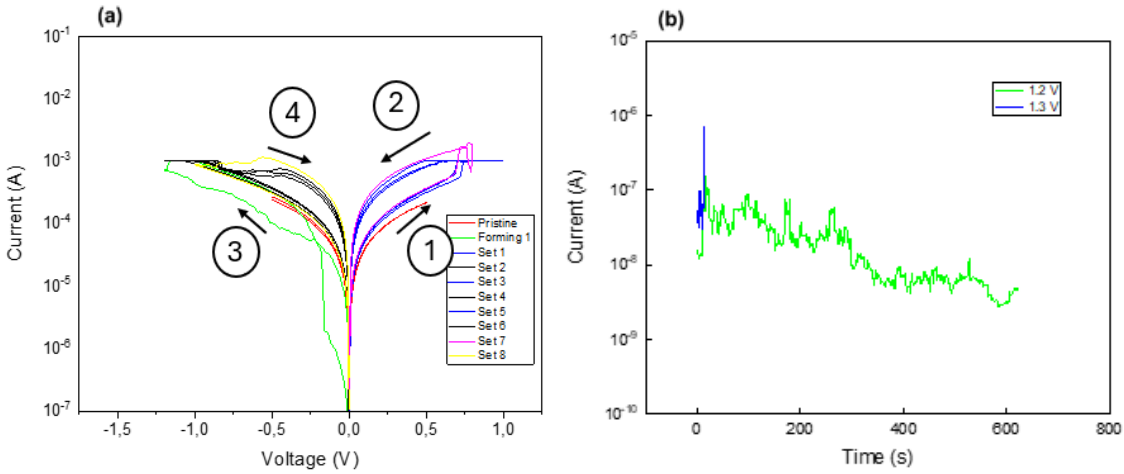

Figure 3-13 **(a)** Switching characteristics of TiPt/Al2O3AlOx /Cu with the AlOx deposition at 300ºC. The device showed thresh-old behaviour repeating the set operation with both positive and negative voltage **(b)** Time to break down test, with fixed 1.2 V and 1.3 V applied to the top contact of the device

After forming was performed, in this case with negative polarity since it showed more stable forming, a series of set test began, concluding that the device operated as a threshold memristor. This evidence is present in the fact that either for a positive voltage and negative the devices went from an

HRS to a LRS. Meaning that they had a volatile behaviour and additionally the creation of the filament could happen on both positive voltage and negative. In order to analysed better the device a soft breakdown test was done. The results are shown in the figures 3-13 and were inconclusive. For these devices, a 1.2V did not provoke soft breakdown while using 1.3V the devices broke down immediate.

3.3.4 Pt/ $Al_2O_3AlO_x$ (150ºC)/Cu

Pristine testing is essential for understanding the initial electrical behavior of memristor devices as a baseline for further analysis. As shown in the figure 3-14, there is a great variation in the pristine state of each device. Some devices exhibited an intrinsic pre-existing state, with conductive filaments already present before testing.

The difference in the initial state of the devices could have originated from the deposition of the AlO_x layer. The non-stoichiometric nature of aluminium oxide, produced by reducing the H_2O precursor time and using lower temperatures that slow reaction rates, led to an uneven oxygen layer distribution. This likely created localized areas with higher oxygen vacancy concentrations, resulting in intrinsic LRS in some devices and HRS in others, which explains the variability observed in the pristine curves. [37]

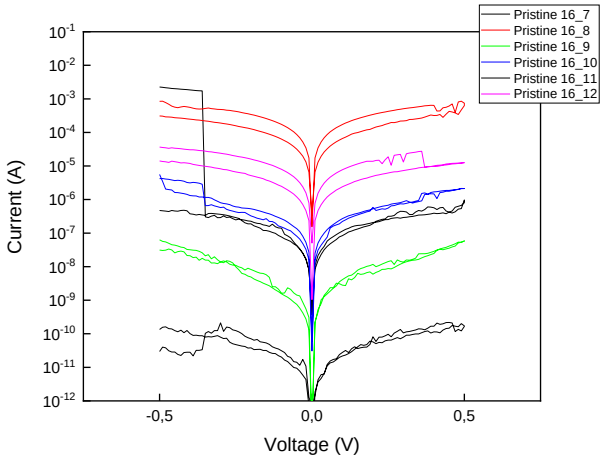

Figure 3-14 Pristine map of Pt/ $Al_2O_3AlO_x$ (150ºC)/Cu devices with a 30 um^2 area. The AlO_x deposition at 150ºC.

The devices were forced to set on the positive side and reset on the negative side. In order to obtain this behaviour, the pristine test was important to determine if the device would need a set forming or reset forming. If in the pristine the device showed to be in the LRS, consider in this case with current levels above 10^{-5} A, a reset forming was performed and in the case of the device to be in the HRS a set forming was performed. In the figures 3-15 (a) and 3-16 (a) we can see an example for each behaviour. However, the results show non-volatile behaviour we can see that after the first reset the difference in conductivity decreased, resulting from an incomplete rupture of the conductive filament.

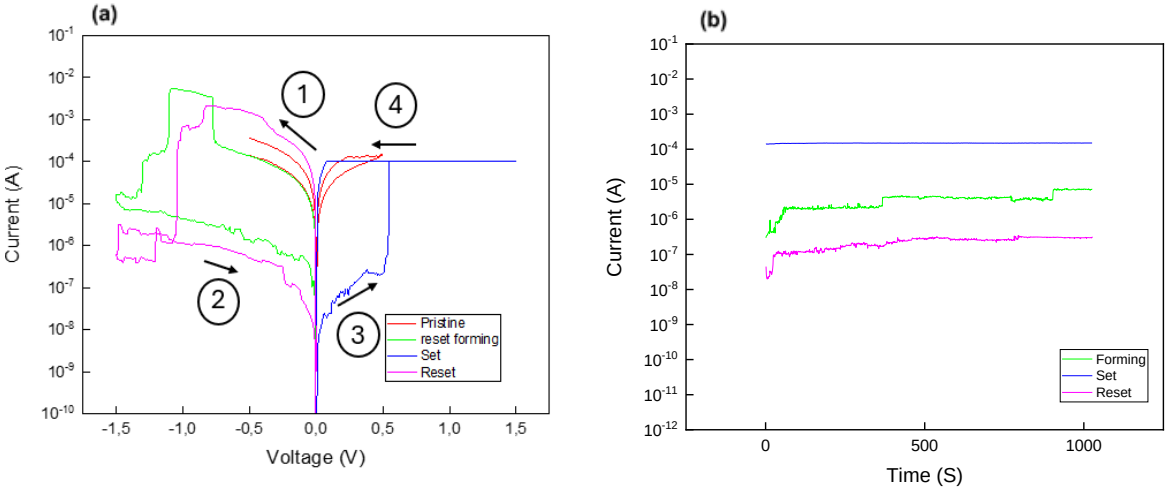

Figure 3-15 **(a)** Reset forming and consequent set **(b)** Retention time test after reset forming on the same device as fig. 3-15 (a)

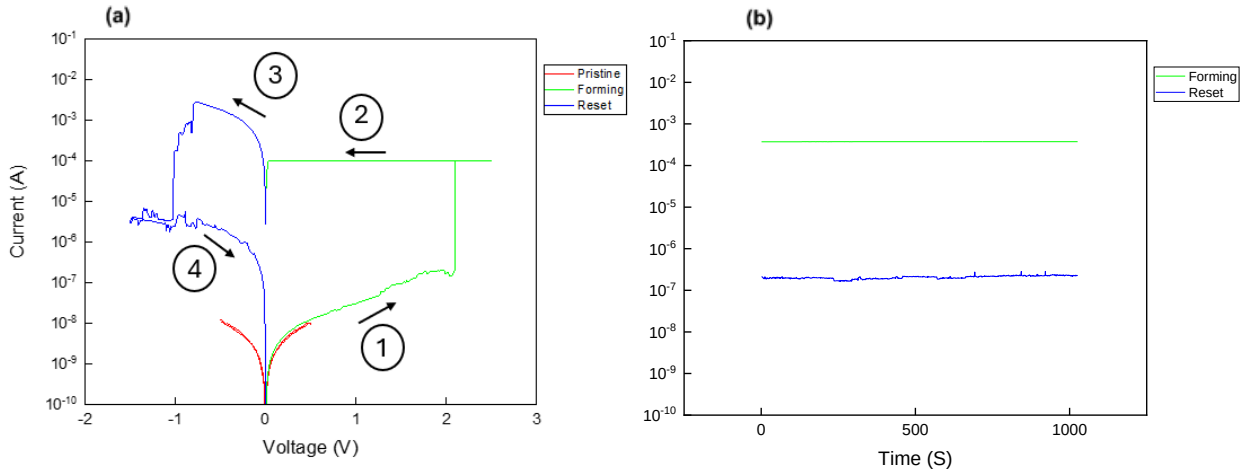

Figure 3-16 **(a)** Set forming and consequent reset **(b)** Retention time test after set forming on the same device as fig 3-16 (a)

The temperature deposition of the AlO_x layer could decrease the defectiveness of the device due to higher reaction rates [37], resulting in a change of the filamentary morphology, from a stable strong filament (figures 3-15 (a) and 3-16 (a), table 3-3) to fragile weak filaments with separated Cu clusters (figure 3-13 (a)).[18]

To further study the switching characteristics of this sample, unipolar tests were performed, since Al_2O_3 devices can display Joule heating effect to switch from HRS to LRS and vice versa. When forming/set/reset was performed with a positive polarity the HRS current significantly decreases while set voltage increases as shown by figure 3-17 (b). The first set done by the device could be during the pristine, since it has an abrupt current variation making the first curve (green) the reset, this could be influence of the area with two high conductive electrodes and the defect AlO_2. Joule heating effect can also occur with negative polarity, so negative unipolar behaviour was tested (figure 3-17 (a)) however, progressively increase of the LRS current was observed, while switching to HRS never occurred.

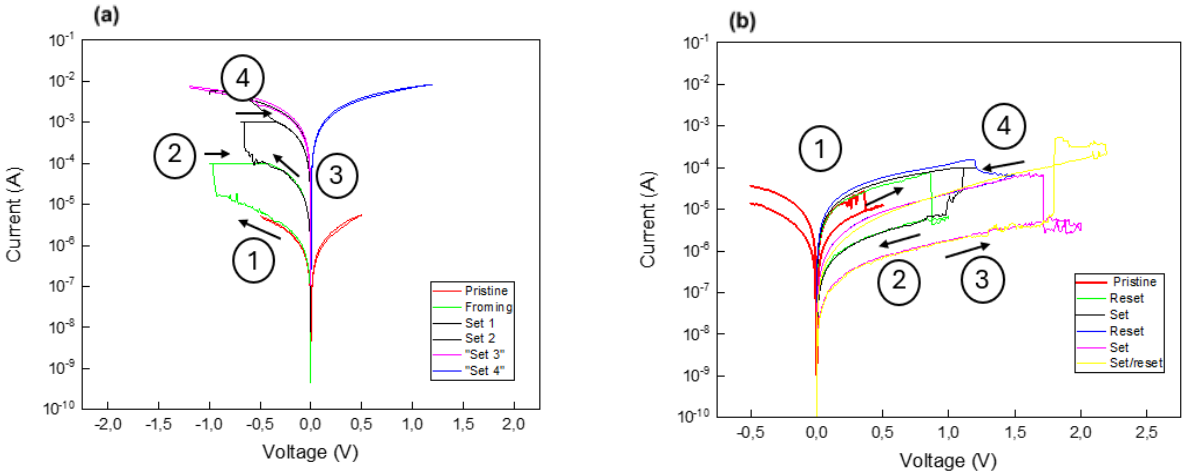

Figure 3-17 **(a)** Negative forming with consecutive increase of the LRS. **(b)** Unipolar device, with positive forming

Another test performed on the devices shown in fig 3-18 demonstrated that some cycling could be obtained by operating as a bipolar memristor with positive forming. A 2,3V voltage applied on the

top electrode initially produced abrupt switching for both forming and reset (table 3-3), when a negative voltage is introduced. As more cycles were performed, analogue set and reset was observed with the current increasing progressively, indicating that the filament formation is slow and controlled. This gradual rise in current results from a higher number of vacancies generated in the dielectric, allowing for more precise control of the device's resistance The gradual reset is attributed to a diffusion-dominated process, where the concentration gradient of oxygen ions controls the rate of filament dissolution. As vacancies are progressively filled, the device's resistance increases gradually, resulting in a smooth transition to the High-Resistance State (HRS).[21], [39]

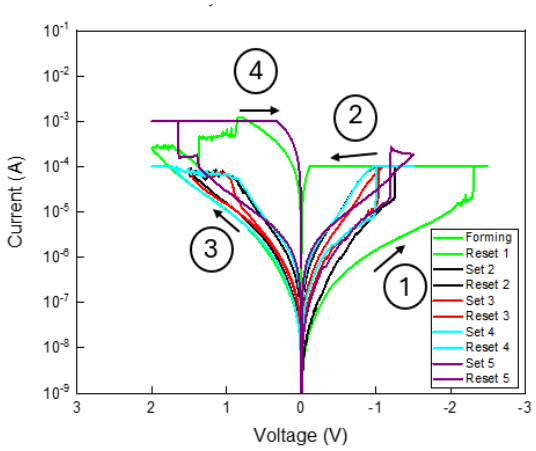

Figure 3-18 Switching characteristics with positive forming and set and reset with opposite polarities.

Table 3-3 Comparison of the results from the third batch

Device Configuration	Vset (V)	Vreset (V)	I-LRS (A)	Vforming (V)	Pristine Range (V)	Retention Time (s)
Pt/Al_2O_3-AlOx (300°C) /Cu	-1.2/0.7	----	10^{-3}	-1.20	[-0.5;0.5]	0
Pt/Al_2O_3-AlOx (150°C) /Cu (fig 3-15)	0.7	-1.5	10^{-4}	-1.5	[-0.5;0.5]	10^3
Pt/Al_2O_3-AlOx (150°C) /Cu (fig 3-16)	---	-1.5	10^{-4}	2.3	[-0.5;0.5]	10^3
Pt/Al_2O_3-AlOx (150°C) /Cu (fig 3-18)	1.2	-2	10^{-3}	2.3	[-0.5;0.5]	----

4

CONCLUSIONS AND FUTURE PERSPECTIVES

4.1 Conclusions

This study focused on optimizing the performance of Al_2O_3-based memristor devices through the exploration of different electrode materials, switching layer configurations, and fabrication processes. The initial configurations using AZO and Al electrodes exhibited poor rectification and unstable switching characteristics, primarily due to the similar work functions of the electrodes, which resulted in ohmic conduction at the interfaces. These post-deposition treatments, such as argon plasma, were insufficient to introduce a substantial number of defects in the Al_2O_3 layer to achieve reliable switching behaviour.

A breakthrough was observed only with the introduction of an AlO_x buffer layer, which significantly enhanced the control over defect formation. This improved defect control facilitated more stable filament formation and dissolution, leading to reliable switching cycles. By XPS, OH-groups possibility related with residual precursor material could be identified as main defect instead of the commonly discussed oxygen deficiency. The optimized Pt/Al_2O_3/ AlO_x /Cu configuration showed improved resistive switching behaviour, offering promising potential for non-volatile memory applications.

The findings underscore the limitations of post-deposition treatments in introducing sufficient defects in Al_2O_3 for stable memristor functionality. Instead, structural modifications like the introduction of a buffer layer are more effective in enhancing performance.

4.2 Future Perspectives

The findings from this study open several avenues for further exploration and optimization of Al_2O_3-based memristor devices. One potential direction involves fine-tuning the thickness and defect density of the switching layers to achieve even more precise control over the set and reset processes. Using multilayer or gradient oxide structures, such as combining Al_2O_3 with other high-k dielectrics or introducing tailored doping elements, could improve the filament formation and dissolution dynamics, enhancing device endurance and retention. Additionally, investigating the role of different electrode materials, particularly those that promote stronger oxygen vacancy formation or diffusion, could lead to further improvements in switching performance and energy efficiency. Moreover, the scalability of these devices for large-scale integration should be explored, particularly in the context of 3D crossbar arrays or neuromorphic computing architectures, where memristors could mimic synaptic functions.

Another promising direction is the integration of Al_2O_3-based memristors with flexible or transparent substrates, broadening their potential applications in wearable electronics, transparent displays, and low-power, edge-computing systems. As memristive technologies mature, combining them with advanced fabrication techniques like atomic layer etching (ALE) or plasma-enhanced ALD (PEALD) could yield devices with enhanced uniformity and performance. Research into the temperature stability of these devices, particularly under harsh environmental conditions, could also pave the way for their use in industrial or space applications. Furthermore, integrating memristors with complementary technologies such as carbon-based materials, quantum dots, or phase-change materials could lead to new hybrid memory architectures, pushing the boundaries of what is possible in terms of speed, energy efficiency, and data storage density.

5 BIBLIOGRAFIA

[1] L. 0 Chua, “Memristor-The Missing Circuit Element,” 1971. doi: 10.1109/TCT.1971.1083337.

[2] D. B. Strukov, G. S. Snider, D. R. Stewart, and R. S. Williams, “The missing memristor found,” *Nature*, vol. 453, no. 7191, pp. 80–83, May 2008, doi: 10.1038/nature06932.

[3] S. Slesazeck and T. Mikolajick, “Nanoscale resistive switching memory devices: A review,” Jun. 11, 2019, *Institute of Physics Publishing*. doi: 10.1088/1361-6528/ab2084.

[4] C. Ye *et al.*, “Physical Mechanism and Performance Factors of Metal Oxide Based Resistive Switching Memory: A Review,” *J Mater Sci Technol*, vol. 32, no. 1, pp. 1–11, Jan. 2016, doi: 10.1016/j.jmst.2015.10.018.

[5] H. Abbas, J. Li, and D. S. Ang, “Conductive Bridge Random Access Memory (CBRAM): Challenges and Opportunities for Memory and Neuromorphic Computing Applications,” May 01, 2022, *MDPI*. doi: 10.3390/mi13050725.

[6] R. Yang, “Review of resistive switching mechanisms for memristive neuromorphic devices,” Sep. 01, 2020, *IOP Publishing Ltd*. doi: 10.1088/1674-1056/aba9c7.

[7] S. Menzel, U. Böttger, M. Wimmer, and M. Salinga, “Physics of the Switching Kinetics in Resistive Memories,” *Adv Funct Mater*, vol. 25, no. 40, pp. 6306–6325, Oct. 2015, doi: 10.1002/adfm.201500825.

[8] F. C. Chiu, “A review on conduction mechanisms in dielectric films,” 2014, *Hindawi Publishing Corporation*. doi: 10.1155/2014/578168.

[9] X. L. Hong, D. J. J. Loy, P. A. Dananjaya, F. Tan, C. M. Ng, and W. S. Lew, “Oxide-based RRAM materials for neuromorphic computing,” Jun. 01, 2018, *Springer New York LLC*. doi: 10.1007/s10853-018-2134-6.

[10] Z. Wang *et al.*, “Memristors with diffusive dynamics as synaptic emulators for neuromorphic computing,” *Nat Mater*, vol. 16, no. 1, pp. 101–108, Jan. 2017, doi: 10.1038/nmat4756.

[11] E. Bär, J. Lorenz, and P. Pichler, “Simulation of Semiconductor Processes and Devices 2016 Edited by.” doi: 10.1109/SISPAD.2016.7605211.

[12] S. M. George, “Atomic layer deposition: An overview,” *Chem Rev*, vol. 110, no. 1, pp. 111–131, Jan. 2010, doi: 10.1021/cr900056b.

[13] N. E. Richey, C. De Paula, and S. F. Bent, “Understanding chemical and physical mechanisms in atomic layer deposition,” Jan. 31, 2020, *American Institute of Physics Inc.* doi: 10.1063/1.5133390.

[14] V. Vandalon and W. M. M. (Erwin) Kessels, “Revisiting the growth mechanism of atomic layer deposition of Al2O3: A vibrational sum-frequency generation study,” *Journal of Vacuum*

Science & Technology A: Vacuum, Surfaces, and Films, vol. 35, no. 5, Sep. 2017, doi: 10.1116/1.4993597.

[15] W. Song *et al.*, "Analog switching characteristics in TiW/Al2O3/Ta2O5/Ta RRAM devices," *Appl Phys Lett*, vol. 115, no. 13, Sep. 2019, doi: 10.1063/1.5100075.

[16] D. Kumar, R. Aluguri, U. Chand, and T. Y. Tseng, "Enhancement of resistive switching properties in nitride based CBRAM device by inserting an Al2O3 thin layer," *Appl Phys Lett*, vol. 110, no. 20, May 2017, doi: 10.1063/1.4983465.

[17] M. Y. Yang *et al.*, "Physical guiding principles for high quality resistive random access memory stack with al2o3 insertion layer," in *Japanese Journal of Applied Physics*, Apr. 2013. doi: 10.7567/JJAP.52.04CD11.

[18] H. Y. Li *et al.*, "Controlled Memory and Threshold Switching Behaviors in a Heterogeneous Memristor for Neuromorphic Computing," *Adv Electron Mater*, vol. 6, no. 8, Aug. 2020, doi: 10.1002/aelm.202000309.

[19] C. F. Chiu, S. Ginnaram, A. Senapati, Y. P. Chen, and S. Maikap, "Switching characteristics and mechanism using al2o3 interfacial layer in al/cu/gdox/al2o3/tin memristor," *Electronics (Switzerland)*, vol. 9, no. 9, pp. 1–16, Sep. 2020, doi: 10.3390/electronics9091466.

[20] S. K. Vishwanath, H. Woo, and S. Jeon, "Enhancement of resistive switching properties in Al2O3 bilayer-based atomic switches: Multilevel resistive switching," *Nanotechnology*, vol. 29, no. 23, Apr. 2018, doi: 10.1088/1361-6528/aab6a3.

[21] X. Zhang *et al.*, "Effect of Joule Heating on Resistive Switching Characteristic in AlOx Cells Made by Thermal Oxidation Formation," *Nanoscale Res Lett*, vol. 15, no. 1, 2020, doi: 10.1186/s11671-019-3229-y.

[22] A. L. J., N. K. T., and J. K.B., "The effect of the top electrode on the switching behavior of bipolar Al2O3/ZnO RRAM," *Microelectron Eng*, vol. 250, Oct. 2021, doi: 10.1016/j.mee.2021.111637.

[23] J. A. Lekshmi, T. N. Kumar, and K. Jinesh, "Multilevel non-volatile memory based on Al2O3/ZnO bilayer device," *Micro Nano Lett*, vol. 15, no. 13, pp. 959–963, Nov. 2020, doi: 10.1049/mnl.2020.0335.

[24] J. Molina *et al.*, "Influence of the surface roughness of the bottom electrode on the resistive-switching characteristics of Al/Al2O3/Al and Al/Al2O3/W structures fabricated on glass at 300 °c," *Microelectronics Reliability*, vol. 54, no. 12, pp. 2747–2753, Dec. 2014, doi: 10.1016/j.microrel.2014.07.006.

[25] A. C. Marques *et al.*, "Stability under humidity, UV-light and bending of AZO films deposited by ALD on Kapton," *Sci Rep*, vol. 9, no. 1, Dec. 2019, doi: 10.1038/s41598-019-54451-0.

[26] S. Salas-Rodríguez, J. Molina-Reyes, J. Martínez-Castillo, R. M. Woo-Garcia, A. L. Herrera-May, and F. López-Huerta, "Modeling of Conduction Mechanisms in Ultrathin Films of Al2O3 Deposited by ALD," *Electronics (Switzerland)*, vol. 12, no. 4, Feb. 2023, doi: 10.3390/electronics12040903.

[27] K. Zhao *et al.*, "Investigation on Transparent, Conductive ZnO:Al Films Deposited by Atomic Layer Deposition Process," *Nanomaterials*, vol. 12, no. 1, Jan. 2022, doi: 10.3390/nano12010172.

[28] K. Miller, K. S. Nalwa, A. Bergerud, N. M. Neihart, and S. Chaudhary, "Memristive behavior in thin anodic Titania," *IEEE Electron Device Letters*, vol. 31, no. 7, pp. 737–739, Jul. 2010, doi: 10.1109/LED.2010.2049092.

[29] H. Kim, M. S. Kim, S. Y. Yoon, and B. J. Choi, "Au/n-InP Schottky diodes using an Al2O3 interfacial layer grown by atomic layer deposition," *Semicond Sci Technol*, vol. 32, no. 2, Jan. 2017, doi: 10.1088/1361-6641/32/2/025011.

[30] H. Lefakis, M. Liehr, G. W. Rubloff, and P. S. Ho, "ALUMINA-Ti INTERFACE REACTIONS STUDIED BY AES AND UPS." doi: 10.1557/PROC-54-133.

[31] Y. Cho *et al.*, "Effect of Electrochemically Active Top Electrode Materials on Nanoionic Conductive Bridge Y2O3 Random-Access Memory," *Nanomaterials*, vol. 14, no. 6, Mar. 2024, doi: 10.3390/nano14060532.

[32] M. Sreng, F. Silva, and P. Roca i Cabarrocas, "In situ Photoluminescence Study of Plasma Effects on Passivation of Crystalline Silicon Coated with Aluminum Oxide," *Physica Status Solidi (A) Applications and Materials Science*, vol. 216, no. 10, May 2019, doi: 10.1002/pssa.201800612.

[33] M. Pereira *et al.*, "Noble-Metal-Free Memristive Devices Based on IGZO for Neuromorphic Applications," *Adv Electron Mater*, vol. 6, no. 10, Oct. 2020, doi: 10.1002/aelm.202000242.

[34] D. S. Kuzmichev, A. A. Chouprik, A. S. Slavich, R. V. Kirtaev, and D. V. Negrov, "Bottom-Electrode Nanoasperities as a Root of the High-Performance Resistive-Switching Effect," *Physica Status Solidi - Rapid Research Letters*, vol. 15, no. 2, Feb. 2021, doi: 10.1002/pssr.202000461.

[35] W. Oepts, M. F. Gillies, R. Coehoorn, R. J. M. Van De Veerdonk, and W. J. M. De Jonge, "Asymmetric bias voltage dependence of the magnetoresistance of Co/Al2O3/Co magnetic tunnel junctions: Variation with the barrier oxidation time," *J Appl Phys*, vol. 89, no. 12, pp. 8038–8045, Jun. 2001, doi: 10.1063/1.1375805.

[36] X. Dong *et al.*, "MoOx Synaptic Memristor with Programmable Multilevel Conductance for Reliable Neuromorphic Hardware," *Journal of Physical Chemistry Letters*, vol. 15, no. 13, pp. 3668–3676, Apr. 2024, doi: 10.1021/acs.jpclett.4c00600.

[37] M. D. Groner, F. H. Fabreguette, J. W. Elam, and S. M. George, "Low-Temperature Al2O3 Atomic Layer Deposition," *Chemistry of Materials*, vol. 16, no. 4, pp. 639–645, Feb. 2004, doi: 10.1021/cm0304546.

[38] V. J. C. Rigi, M. K. Jayaraj, and K. J. Saji, "Envisaging radio frequency magnetron sputtering as an efficient method for large scale deposition of homogeneous two dimensional MoS2," *Appl Surf Sci*, vol. 529, Nov. 2020, doi: 10.1016/j.apsusc.2020.147158.

[39] B. Sarkar, B. Lee, and V. Misra, "Understanding the gradual reset in Pt/Al2O3/Ni RRAM for synaptic applications," *Semicond Sci Technol*, vol. 30, no. 10, Aug. 2015, doi: 10.1088/0268-1242/30/10/105014.

[40] J. A. Lekshmi, T. N. Kumar, and K. Jinesh, "Multilevel non-volatile memory based on Al2O3/ZnO bilayer device," *Micro Nano Lett*, vol. 15, no. 13, pp. 959–963, Nov. 2020, doi: 10.1049/mnl.2020.0335.

[41] H. Idriss, “On the wrong assignment of the XPS O1s signal at 531–532 eV attributed to oxygen vacancies in photo- and electro-catalysts for water splitting and other materials applications,” Oct. 01, 2021, *Elsevier B.V.* doi: 10.1016/j.susc.2021.121894.